ENVIRONMENTAL RESEARCH
LETTERS

LETTER • OPEN ACCESS

Spatial variation and seasonal dynamics of leaf-area index in the arctic tundra-implications for linking ground observations and satellite images

To cite this article: Sari Juutinen *et al* 2017 *Environ. Res. Lett.* **12** 095002

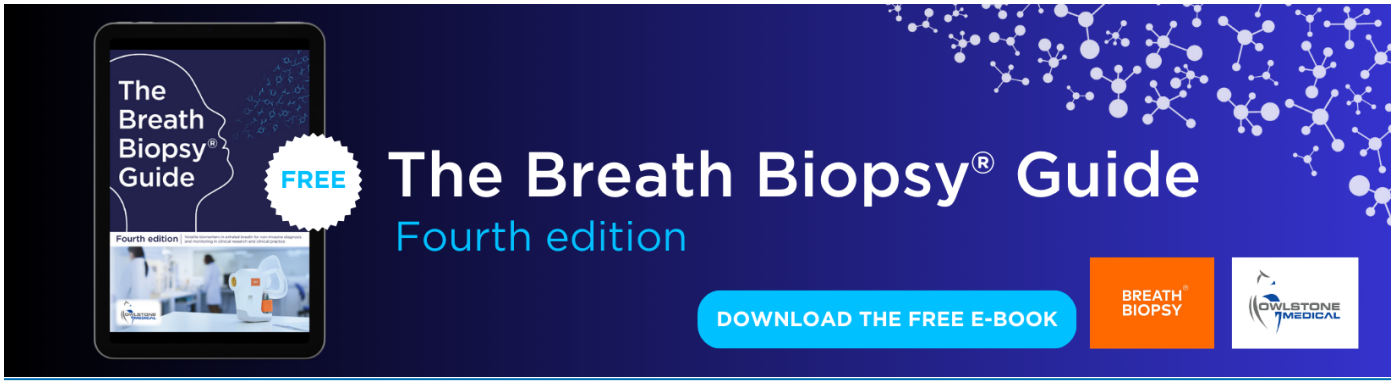

Environmental Research Letters

LETTER

Spatial variation and seasonal dynamics of leaf-area index in the arctic tundra-implications for linking ground observations and satellite images

Sari Juutinen[1,5], Tarmo Virtanen[1], Vladimir Kondratyev[2], Tuomas Laurila[3], Maiju Linkosalmi[3], Juha Mikola[4], Johanna Nyman[1], Aleksi Räsänen[1], Juha-Pekka Tuovinen[3] and Mika Aurela[3]

[1] Department of Environmental Sciences, University of Helsinki, PO Box 65 (Viikinkaari 1), FI-00014 University of Helsinki, Helsinki, Finland
[2] Yakutian Service for Hydrometeorology and Environmental Monitoring, Tiksi, Russia
[3] Finnish Meteorological Institute, PO Box 503, FI-00101 Helsinki, Finland
[4] Department of Environmental Sciences, University of Helsinki, Niemenkatu 73, 15140 Lahti, Finland
[5] Author to whom any correspondence should be addressed.

E-mail: sari.juutinen@helsinki.fi

Keywords: arctic, multispectral, LAI, VHSR, vegetation

Supplementary material for this article is available online

OPEN ACCESS

RECEIVED
16 February 2017

REVISED
11 July 2017

ACCEPTED FOR PUBLICATION
13 July 2017

PUBLISHED
23 August 2017

Abstract

Vegetation in the arctic tundra typically consists of a small-scale mosaic of plant communities, with species differing in growth forms, seasonality, and biogeochemical properties. Characterization of this variation is essential for understanding and modeling the functioning of the arctic tundra in global carbon cycling, as well as for evaluating the resolution requirements for remote sensing. Our objective was to quantify the seasonal development of the leaf-area index (LAI) and its variation among plant communities in the arctic tundra near Tiksi, coastal Siberia, consisting of graminoid, dwarf shrub, moss, and lichen vegetation. We measured the LAI in the field and used two very-high-spatial resolution multispectral satellite images (QuickBird and WorldView-2), acquired at different phenological stages, to predict landscape-scale patterns. We used the empirical relationships between the plant community-specific LAI and degree-day accumulation (0 °C threshold) and quantified the relationship between the LAI and satellite NDVI (normalized difference vegetation index). Due to the temporal difference between the field data and satellite images, the LAI was approximated for the imagery dates, using the empirical model. LAI explained variation in the NDVI values well ($R^2_{adj.}$ 0.42–0.92). Of the plant functional types, the graminoid LAI showed the largest seasonal amplitudes and was the main cause of the varying spatial patterns of the NDVI and the related LAI between the two images. Our results illustrate how the short growing season, rapid development of the LAI, yearly climatic variation, and timing of the satellite data should be accounted for in matching imagery and field verification data in the Arctic region.

Introduction

Vegetation monitoring is a tool for detecting the impacts of climate change on the composition and phenology of arctic ecosystems. For example, satellite image series spanning several decades have already revealed the large-scale greening of the arctic, a consequence of the increased plant growth and spatial expansion of shrubs and trees (Stow *et al* 2004, Forbes *et al* 2010, Frost and Epstein 2014). Spatially extensive observations of vegetation are equally essential when vegetation parameters, such as the leaf-area index (LAI), are included in ecosystem models (e.g. Cramer *et al* 2001, Melton *et al* 2013). Many key properties of vegetation can be reasonably well inferred from spectral reflectance and thus mapped for large areas, using remotely sensed data (Laidler and Treitz 2003, Laidler *et al* 2008, Ustin and Gamon 2010). However, the temporal and spatial scales of currently available remote-sensing products may pose a challenge during

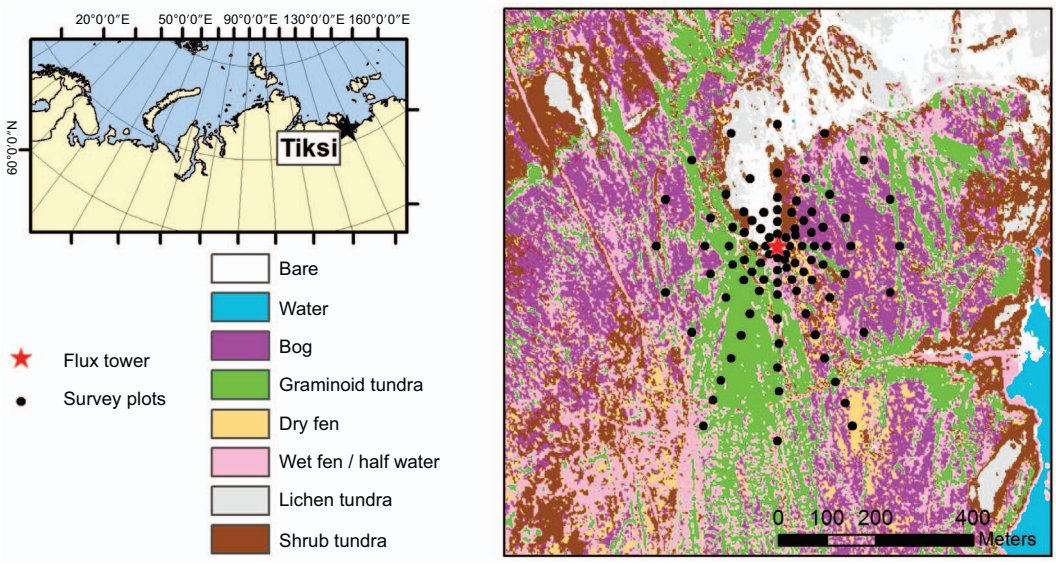

Figure 1. Location of Tiksi (left) and the land-cover map of the study area with survey plot locations (right). The graminoid tundra and flood meadow were grouped in the land-cover classification.

mapping of spatially heterogeneous landscapes, such as the northern tundra (Virtanen and Ek 2014).

The pixel size of the commonly used satellite imageries, e.g. those obtained from the Landsat and Moderate Resolution Imaging Spectroradiometer (MODIS) satellites, ranges from tens to hundreds of meters and cannot reveal fine-scale heterogeneity in vegetation and ecosystem properties (Laidler *et al* 2008, Virtanen and Ek 2014, Mora *et al* 2015, Bratsch *et al* 2016). This complicates the examination of plant growth responses to warming, which may vary among neighboring communities (e.g. McManus *et al* 2012, Bratsch *et al* 2016). To resolve this problem, images of very high spatial resolution (VHSR, 0.3−2 m pixel size) have become available in recent years. Their usage, however, is hampered by the high price, limited temporal availability, which is caused by the relatively long revisit periods of high-resolution image sensor satellites in the same location, and by the frequent cloud cover and low solar angle in the Arctic (Hope and Stow 1996, Rees *et al* 2002, Stow *et al* 2004, Westergaard-Nielsen *et al* 2013). Therefore, the best-quality image often does not temporally match the ground-truth data.

This temporal mismatch is a source of uncertainty in the end product, because the reflectance is dependent on the amount of biomass, plant species composition, and the water, nutrient, and pigment contents of plant tissues, all of which are affected by the growth stage of the vegetation (e.g. Ustin and Gamon 2010). Therefore, the spectral responses to the seasonal changes in vegetation properties should be better understood (Garrigues *et al* 2008, Ustin and Gamon 2010, Rautiainen *et al* 2011, Westergaard-Nielsen *et al* 2013). Since the growing season is short and the changes in the LAI and biomass of the vegetation are rapid in the Arctic, it is likely that even a small time difference between the image and the ground-truth data can result in wide variations in terms of growth stage.

In this study, therefore, our objective was to quantify the spatial and seasonal variation in LAI among the dominant plant communities in the arctic tundra and to evaluate how the seasonality of the vegetation affects the interpretation of vegetation structure from satellite images. We measured the seasonal development and spatial pattern of the LAI in the coastal arctic tundra near Tiksi, NE Russia, in the summer of 2014 and examined how the normalized difference vegetation index (NDVI), derived from the reflectance data, varied among the plant communities and between the VHSR multispectral satellite images of two different growing seasons. To quantify the dependence of the seasonal LAI development on the weather and for reconstructing the LAI values, we developed regression models between the LAI, degree-days (DD) accumulation, and satellite-based NDVI. Based on these models, we then evaluated the impacts that the temporal mismatch between the satellite imagery and field data may have on the interpretation of the NDVI and LAI distributions in the landscape.

Methods

Study site

The study site is located about 500 m from the coast of the Arctic Ocean near the Hydrometeorological Observatory of Tiksi in NE Russia (71.5936°N, 128.8850°E, figure 1). The climate at Tiksi is arctic, with very cold and windy winters, short but relatively warm summers, and short shoulder seasons between these. The mean annual temperature was −12.7 °C and the mean annual precipitation 323 mm in

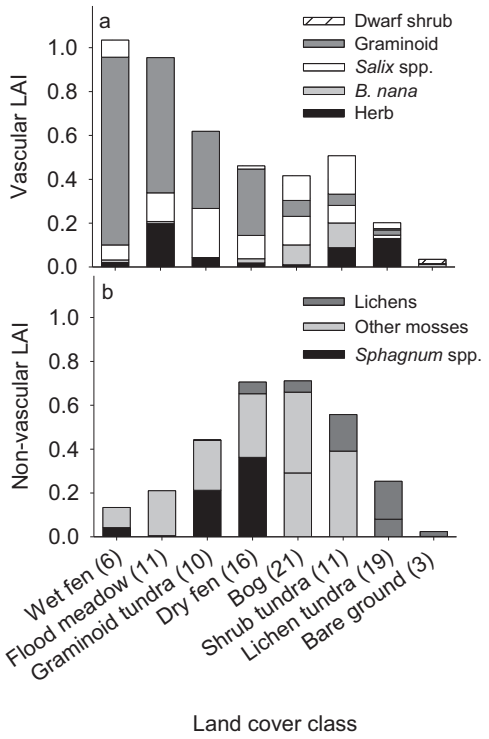

Figure 2. Mean leaf-area index (LAI) of (*a*) all vascular plants and (*b*) all non-vascular plants in the various land cover classes (LC). In both cases, the LAI is divided into plant functional types, while the LCs are shown in order of decreasing wetness from the left (the number of harvested field plots in each type is given in parentheses).

1981–2010. Within this reference period, the average growing season (0 °C threshold) lasted from 7 June to 26 September, with DD of 668 (Arctic and Antarctic Research Institute AARI 2016). Meteorological data from the Hydrometeorological Observatory was used to calculate the DD for the examined periods in this study.

The site represents a typical coastal tundra of Eastern Siberia with alkaline bedrock and high plant species diversity. We focused on an area of approximately 1 km^2 around the micrometeorological station, established in 2010 for eddy covariance (EC) measurements of the land-atmosphere exchange of water, heat, carbon dioxide (CO_2), and methane (CH_4) (Uttal *et al* 2016, figure 1). The terrain around the EC mast was relatively flat; in addition to microtopographic variation there was a gentle slope rising towards the north and a small stream running through the area. The vegetation and land-cover types within the area were classified, using ground-based visual judgement during an expedition in 2012. These land cover classes (LC) were characterized as (1) dry fen, (2) wet fen, (3) bog, (4) lichen tundra, (5) shrub-moss tundra, (6) graminoid tundra, (7) flood meadow, (8) bare ground, and (9) water.

The fen and bog were peat-forming environments, while the other land cover classes showed no clearly discernible peat. Sedges (*Carex* L. spp.) characterized the vascular plant vegetation in the fens (figure 2). Sphagnum mosses (*Sphagnum* L.) and feathermosses (e.g. *Pleurozium schreberi* (Willd. ex Brid.) Mitt) with shrubs were abundant in the dry fens, while the moss cover was sparse, due to aboveground water in the wet fens. The bogs showed typical microtopographic variation, and their vegetation was characterized by the presence of dwarf shrubs, dwarf birch (*Betula nana* L.), *Sphagnum*, and feathermosses. The vegetation of the flood meadows along the stream and drier graminoid tundra was dominated by graminoids (sedges, grasses) and willows (*Salix* L. spp.). Abundant feathermoss coverage on the ground layer and dwarf shrubs in the field layer characterized the shrub-moss tundra. Lichen tundra patches alternated with stony bare-ground surfaces.

Flow of the study

Several steps were needed to obtain time series of LAI, to model LAI for each land cover class (LC) for the years of satellite data, and to produce the LAI maps over the study area. The steps were, in brief, as follows, while the details are given in following paragraphs.

1. Phenological dynamics of vegetation: Vegetation surveys (% cover and mean height of each plant functional types) in sample of plots seven times over the study period in 2014.
2. Estimation of LAI on basis of % cover and height: Sample of plots were harvested after vegetation survey during the peak biomass and LAI of harvested material was measured at PFT level. Data were used to develop regression models to predict LAI.
3. Producing time series of total and vascular plant LAI: A model using degree-day accumulation and chilling temperature accumulation as drivers was fitted for each land cover class and LAI was modelled for years 2005, 2012, and 2014.
4. Mapping spatial distribution of LAI using satellite data: LAI was modeled over the study area using relationship between satellite derived NDVI and LAI in the study plots.

Field data

The field data on the vegetation were collected in the summer of 2014, which had a warmer (871 DD) growing season than the long-term average. The 92 inventory plots with radius of 2.5 m were placed along 16 compass points at regular distances of 25, 50, 75, 100, 150, and 250 m from the EC mast (figure 1). Several additional plots were monitored at distances of 300, 350, and 400 m to balance the number of plots in the various LCs. In each plot, the vegetation was inventoried in four subplots (45 cm × 45 cm in area), located 2 m from the plot midpoint in four main compass directions. Each plot was classified according

Table 1. Regression models describing the dependence of the leaf-area index (LAI) of the various plant functional types on their areal cover (C, %) and height (H, cm) in the Tiksi field plots surveyed in 2014. All regressions and parameters were significant at $p < 0.05$.

Plant functional type		*df* reg., res.[a]	R^2_{adj}[b]
Salix spp.	$LAI = 0.0126 \times C$	1, 63	0.88
Dwarf shrub	$LAI = 0.0192 \times \sqrt{(C + 0.001)} + 0.0397 \times H$	2, 63	0.93
Betula nana	$LAI = 0.0132 \times C$	1, 36	0.91
Graminoids	$LAI = 0.0150 \times C$	1, 85	0.88
Herbs	$LAI = 0.0098 \times C + 0.0046 \times H$	2, 84	0.93

[a] Degrees of freedom for regression and residuals.
[b] Adjusted coefficient of determination.

to the *a priori* LC scheme described above (dry fen, wet fen, etc.), and the plot midpoint was georeferenced, using a Global Positioning System (GPS) device and a measuring tape to achieve a location accuracy of 1–3 m.

The vegetation was surveyed to characterize the species composition and to quantify the LAI and its seasonal development in the various LCs of the tundra. The vegetation was inventoried as plant functional types (PFTs), following the typification by Hugelius *et al* (2011), which is a modification of that by Chapin *et al* (1996). The PFTs included: (1) Sphagnum mosses, (2) other mosses, (3) lichen (4) dwarf shrubs, (5) deciduous shrub *Betula nana*, (6) deciduous shrub *Salix* spp., (7) herbaceous species, and (8) graminoids.

The projection cover percentage of each PFT was visually estimated, and the mean height was measured in each of the subplots during the main survey, 23–24 July 2014. These values were then averaged for the main 2.5 m radius plot to relate the vegetation and the satellite image-based spectral reflectance. The seasonal development of the vegetation in one of the subplots was monitored by seven successive surveys performed between 2 July and 15 August 2014. Another subplot was harvested immediately after the main survey to quantify the one-sided LAI. The vascular plant material harvested was scanned, using a Canon MP Navigator EX scanner (Canon Inc., Tokyo, Japan) and by calculating the green surface area (= LAI) of the scanned images, using GNU Image Manipulation Program 2 (GIMP 2) software. The LAI of the mosses was estimated as a projection coverage, i.e. we determined that a 100% cover would represent an LAI of 1 (Riutta *et al* 2007). This approach underestimates the true multilayered leaf area of mosses, but probably estimates reasonably well their light-capturing and reflectance properties, due to the lower pigment and nutrient contents in moss tissues (Tieszen and Johnson 1968, Moore *et al* 2006, Street *et al* 2012). Using the data of the harvested subplots, we then calculated for each PFT the relationship between the areal cover, plant height, and LAI and, using these relationships, estimated the LAI for each subplot at the time of the main survey (table 1). These relationships were also used, assuming space-for-time substitution, to estimate the LAI for the subplots that were monitored for seasonal dynamics.

Satellite image acquisition and processing

To examine the spatial and temporal variation in the vegetation patterns within the study area, we acquired two VHSR multispectral satellite images from the archive of DigitalGlobe (Westminster, CO, USA). To enable the comparison of images taken under different atmospheric conditions, the images were corrected for atmospheric scattering and transformed into surface reflectance values, using the dark-object subtraction method (Chavez 1988).

The images, QuickBird (QB, DigitalGlobe, 15 July 2005) and WorldView-2 (WV2, DigitalGlobe, 12 August 2012), were chosen because they were of good quality and showed the best temporal matching with the collection of the peak season field verification data (23–24 July 2014) in terms of calendar days. The growing season of the QB image was shorter and cooler (10 June–30 September 2005, 646 DD) than the growing seasons of the WV2 image (22 May–30 September 2012, 1071 DD) and the verification data (6 June–24 September 2014, 863 DD). Thus, the QB image captured a period during which the vegetation was in the fast-growing phase, while the WV2 image captured the peak LAI period (figure 3 (*a*)–(*c*)).

The mean reflectance values were extracted for circular plots with a 2.5 m radius. The reflectance data were used to calculate the normalized difference vegetation index, NDVI = (NIR − VIS)/(NIR + VIS), which describes the absorbance of the red portion of visible (VIS) light and the reflectance of near-infrared (NIR) radiation by green vegetation. Thus, the NDVI is an indicator of the quantity and photosynthetic capacity of green vegetation and has commonly been used in spatial extrapolations of LAI (Tucker 1979, Laidler and Treitz 2003, Shaver *et al* 2013). Supervised land-cover classification was carried out, based on a WV2 image (12 August 2012) to visualize the spatial distribution of vegetation in the area (figure 1).

Temporal modeling of the LAI

We examined the factors determining the seasonal development of the LAI to estimate it for the specific dates of the two satellite images. Since our field data on

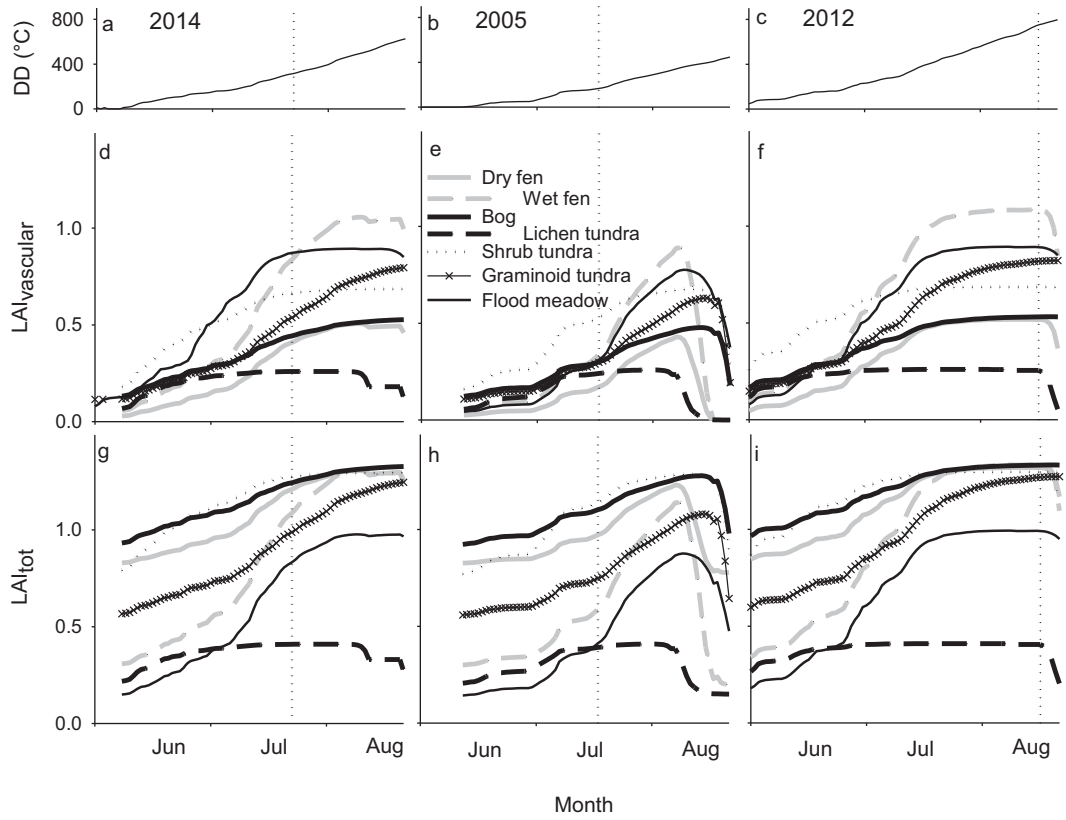

Figure 3. Accumulation of (*a*)−(*c*) the temperature sum above 0 °C (degree-days, DD), (*d*)−(*f*) vascular plant leaf-area index (LAI), and (*g*)−(*i*) total LAI in the dominant plant community types for the years of the field data (2014), QuickBird (QB) image (2005), and WorldView-2 (WV2) image (2012). The vascular plant LAI was modeled based on seasonal accumulated temperature (DD) (table 2), while the non-vascular LAI was assumed to be constant and directly proportional to the areal cover. The vertical dotted lines indicate the timing of the satellite images and of the field data.

LAI development originated from a single growing season only, we used long-term (years 2010–2014) data on the daily maximum ecosystem photosynthesis (GP_{max}) to define a functional form that describes the seasonal growth of vegetation from soil thawing to maximum activity and further to senescence. This approach is justified by the close relationship between the LAI and GP_{max} (e.g. Laurila *et al* 2001, Street *et al* 2007). The daily GP_{max} was derived from the continuous CO_2 flux data measured with the EC method at the site. The GP_{max} was determined from the eddy covariance flux as the night-day difference in net ecosystem CO_2 exchange (NEE). The daily GP_{max} was obtained as the difference of the 7 day running mean of the nighttime NEE (photosynthetic photon flux density < 20 μmol m^{-2} s^{-1}) and 3 day running mean of the daytime NEE (PPFD > 600 μmol m^{-2} s^{-1}). A function including two temperature-dependent sigmoid terms operating during different phases of the growing season proved suitable for modeling the GP_{max} cycle (supplement 1 available at stacks.iop.org/ERL/12/095002/mmedia). It was fitted to the LAI data

$$\mathrm{LAI}(t) = a\left[\frac{1}{1+\exp\left(-\frac{S_1(t)-b_1}{c_1}\right)} - \frac{1}{1+\exp\left(-\frac{S_2(t)-b_2}{c_2}\right)}\right] \quad (1)$$

In this equation, t is the time, S_1 is the DD accumulated from all daily mean air temperatures *over* 0 °C, and S_2 is the DD accumulated during the latter part of the growing season (after 15 July) from the daily mean air temperatures above 0 °C, but below 10 °C and a, b_1, b_2, c_1, and c_2 are the parameters to be estimated. The equation was fitted to the total vascular plant LAI data for each LC (table 2). The fits obtained were favorable for the period covered by field observations in 2014, and the values outside the measurement period (2 July–15 August) were not used in any further analysis.

Data analysis

A paired sample Wilcoxon signed-rank test was used to determine whether the vegetation classes showed significant seasonal differences in their NDVI signals; i.e. the $NDVI_{QB}$ (15 July 2005) and $NDVI_{WV2}$ (12 August 2012) were paired for each PCT. To further illustrate the seasonal changes in the various plant communities, we calculated the difference in NDVI between the late-season and early-season image ($NDVI_{WV2}-NDVI_{QB}$). The relationships between the LAI (either measured in the 2014 field survey or estimated for the actual dates of the satellite images) and the NDVI derived from the QB and WV2 images were examined, using regression analysis. This relationship is commonly used to extrapolate the

Table 2. Fit statistics and parameter values of the vascular plant leaf-area index (LAI) model (equation (1)) for each land cover class. The model was fitted to the community mean LAI of 7 measurement days.

Land cover class	R^2_{adj} [a]	RMSE [b]	a	b_1	c_1	b_2	c_2
Wet fen	0.98	0.055	1.09	227	74	153	9
Flood meadow	0.96	0.077	0.90	212	70	200	20
Dry fen	0.97	0.032	0.52	220	74	150	9
Graminoid tundra	0.96	0.063	0.83	241	126	200	9
Bog	0.95	0.032	0.53	138	113	200	9
Shrub tundra	0.76	0.045	0.69	83	68	200	9
Lichen tundra	0.63	0.032	0.26	58	43	130	9

[a] Adjusted coefficient of determination.
[b] Root-mean-squared error.

LAI over a landscape, using the NDVI as input (e.g. Shaver *et al* 2007, Williams *et al* 2008, Shaver *et al* 2013, Marushchak *et al* 2013). The regression relationships for both the total and vascular LAI were applied to calculate the LAI maps, using the QB and WV2 images. We used IBM SPSS Statistics Version 22 (IBM Corp., Armonk, NY, USA) and JMP Pro 10.02 software (SAS Institute Inc., Cary, NC, USA) for statistical modeling and testing.

Results

At harvest time, the average vascular plant LAI was 0.55 across all the harvested plots. The highest values were found in the wet fen and flood meadow, both dominated by graminoids, while the lichen and bare-ground tundra showed the lowest values (figure 2(*a*)). The moss LAI was highest in the dry fen and bog (figure 2(*b*)). The total LAI did not differ greatly among the LCs, excluding the lichen and bare-ground tundra, due to the contrasting distribution of mosses and vascular plants in the communities.

The seasonal amplitudes of the vascular and total LAIs was largest in those communities with abundant graminoid vegetation, i.e. in the wet fen, graminoid tundra and flood meadow (figures 3(*d*)−(*i*). Our modeled LAI showed that the development of the vegetation was delayed in the cool growing season of 2005 (figures 2(*e*) and (*h*)), whereas in 2012 the LAI developed rapidly, due to the early start of the growing season and higher DD accumulation (figures 3(*c*), (*f*) and (*i*)). The yearly differences were pronounced in the graminoid-dominated communities and small in the moss- and evergreen-dominated communities (3(*d*)−(*f*)). The varying meteorological conditions during the years of the satellite images led to differences in the LAI that were larger than would be expected, based solely on the difference between the dates of the images.

The differences in the LC-specific NDVI values between the two satellite images were in line with the differences in vegetation development illustrated by the LAI. In the QB image, which represents the LAI in the growth phase (figure 4(*a*)), the NDVI values were largest in the shrub-moss tundra and bog, whereas in the WV2 image, which represents the maximum LAI, the NDVI maxima were found in the wet fen, flood meadow, and graminoid tundra (figure 4(*b*)). The median difference in the $NDVI_{QB}$ and $NDVI_{WV2}$

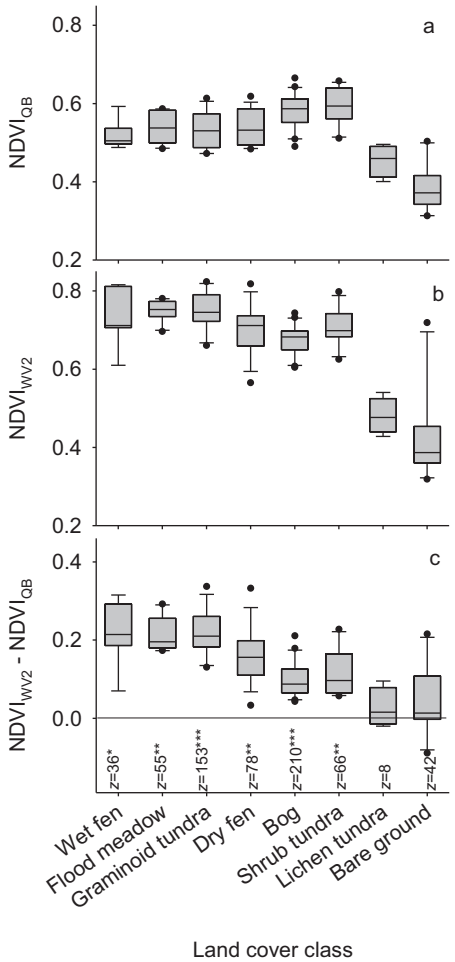

Figure 4. Boxplots of the normalized difference vegetation index (NDVI) derived from the (*a*) QuickBird (QB) and (*b*) WorldView-2 (WV2) reflectance, and (*c*) the difference between these for the various land cover classes (shown in order of decreasing wetness from the left). The horizontal line, box, and whisker ends indicate the median, 25th and 75th percentiles, and the 10th and 90th percentiles, respectively, and the data points outside this range are shown by dots. The *Z*- and *p*-statistics of the Wilcoxon signed-rank test of the difference between the early (QB image) and late-season (WV2 image) NDVI in the various land cover classes are shown in panel (*c*) $*p < 0.05$, $**p < 0.01$, $***p < 0.001$.

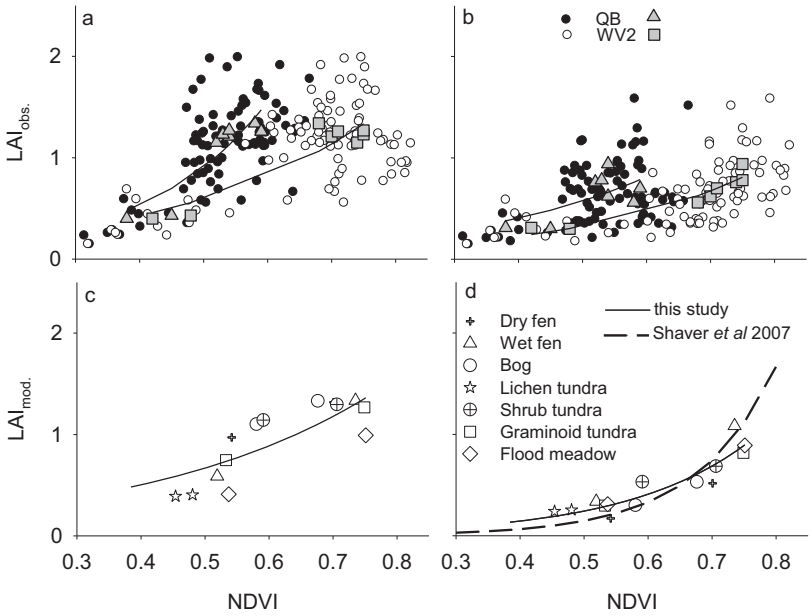

Figure 5. Relationships between normalized difference vegetation index (NDVI) and the field data of (*a*) the total leaf-area index (LAI) and (*b*) vascular plant LAI, with the NDVI derived from the QuickBird (QB) and WorldView-2 (WV2) satellite images, i.e. comparing LAI observations from 2014 with NDVI from 2005 and 2012. The open and closed circular data points denote individual study plots, while the land cover class means are indicated by the gray triangle and square symbols. For the regressions, the community means were used as dependent variables: LAItot = 0.06 e(5.34×$NDVI_{QB}$), $R^2_{adj.}$ = 0.81, LAItot = 0.12 e(3.24×$NDVI_{wv2}$, $R^2_{adj.}$ = 0.86, LAIvasc = 0.1 e(3.48×$NDVI_{QB}$), $R^2_{adj.}$ = 0.42, and LAIvasc = 0.05 e(3.36×$NDVI_{wv2}$), $R^2_{adj.}$ = 0.92. The relationships between the NDVI and (*c*) total LAI and (*d*) vascular plant LAI, modeled to temporally match the QB and WV2 images. The data points represent the land cover class means and the regressions show are: LAItot = 0.1 e(2.83×NDVI), $R^2_{adj.}$ = 0.65 and LAIvasc. = 0.02 e (5.18×NDVI), $R^2_{adj.}$ = 0.84. LAI_{mod} = modeled LAI, LAI_{obs} = observed LAI. Equation (LAI = 0.0026×$e^{8.0783\times NDVI}$) presented in Shaver *et al* (2007 and 2013) also shown in the paned (*d*).

values was significantly different from zero for all the plant communities, except for the lichen tundra and bare ground, which showed equally low NDVI values in both images (figure 4(*b*) and (*c*)). The NDVI differences were larger among the LCs in the WV2 image than in the QB image.

The relationship between the NDVI and LAI showed a typical exponential shape with reasonably favorable adjusted coefficients of determination (R^2_{adj} = 0.42–0.92, $p > 0.05$). The regression parameters, however, varied depending on the satellite image used due to the different timing of the images in relation to the field data and growth stage (figure 5(*a*) and (*b*)). The variation in total and vascular plant LAI was better explained by the $NDVI_{WV2}$ than the $NDVI_{QB}$, due to the growth stage in the WV2 image better resembling the growth stage in the field data (figure 3). To illustrate the spatial variation of the LAI in the study area at the time of the satellite images, we calculated the NDVI-LAI regressions, using values adjusted with the phenological model (figure 5(*c*) and (*d*)). For vascular LAI the relationship was roughly agreeable with a spatially more representative transfer function in Shaver *et al* (2007, 2013) based on multiple arctic sites (figure 5(*d*)). In the scale of whole focus area particularly the vascular LAI differed between the images. In the WV2 image, the average vascular LAI was 30% higher and the graminoid LAI in the graminoid communities was 2.3–2.9 f old compared to their respective values in the QB image (figure 6).

Discussion

In this study, we documented the spatial and temporal patterns of the LAI in the low-growth vegetation of the coastal arctic tundra and generalized these observations for the entire study area, using VHSR satellite images. Our study illustrates the impact of the spatial and temporal variation in the seasonality of vegetation, measured as the LAI, on the inference of remote-sensing products in the tundra. Interestingly, both the plant communities and the LAI showed substantial small-scale spatial variation in our study area, which appears to be typical of tundra landscapes (Marushchak *et al* 2013, Virtanen and Ek 2014). The temporal dynamics of the LAI also differed among the plant communities. The graminoid-dominated vegetation showed intensive growth within the short arctic summer, leading to a large seasonal amplitude in the LAI. In the *Carex*-dominated wet fens and flood meadows, the sparse moss cover further amplified these seasonal differences in total greenness. The mixed vegetation of the evergreen and deciduous dwarf shrubs showed a smaller vascular plant LAI and a more abundant moss cover and thus less seasonal variation in its NDVI (figures 2 and 3). These differences in the LAI and NDVI dynamics were driven by the variation in the overwintering green biomass and leaf production dynamics among the various PFTs. Graminoids have little overwintering green biomass, while the evergreen dwarf shrubs show rapid

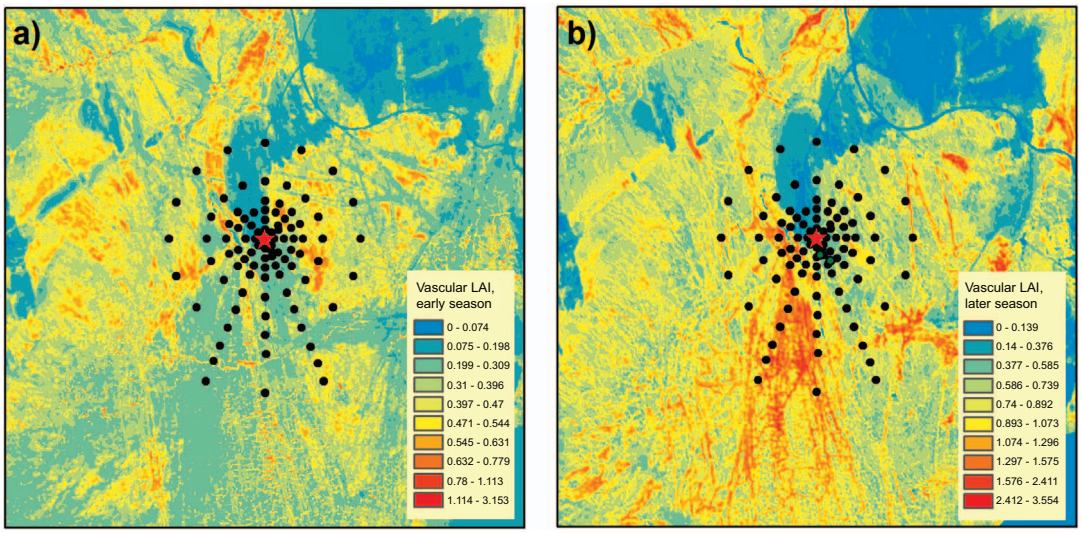

Figure 6. Spatial extrapolation of the vascular plant leaf-area index (LAI), based on the normalized difference vegetation index (NDVI) from the QuickBird (QB) and WorldView-2 (WV2) images representing stages of a) increasing and b) peak LAI. The images were taken on 15 July 2005 and 12 August 2012, respectively. See figure 5(*c*) for the equation used to calculate the LAI and figure 1 for the distribution of the vegetation types.

green-up in the spring and gradual leaf turnover during the late summer (Johnson and Tieszen 1976, Saarinen 1998, Street *et al* 2007, Maanavilja *et al* 2010). Mosses, in turn, show little seasonal variation in nutrient and pigment contents (Moore *et al* 2006, Street *et al* 2012), but their water content affects their reflective properties (Vogelmann and Moss 1993).

We applied a simple regression model to estimate the interannual variation in the seasonal LAI development and to match the phenological phases of the LAI illustrated in the two satellite images. The images were taken in different years and were −9 and +19 ordinal days apart from the date of the field data collection, which in turn represented the peak LAI season (figure 3). Both the NDVI values extracted for the survey plots and the modeled LAI values indicated that the earlier, i.e. −9 days, image represented a phase of vegetation development in which the graminoid LAI had not yet reached its growing season maximum (figures 3 and 4). Apparently, despite a larger deviation in the number of ordinal days, the later image was similar to the field data in terms of the growth phase.

We acknowledge modeling the LAI values for years with no field measurements, but the continuous data of daily GP_{max} that we have available for 2010–2014 (S1) and the robust correlation between the LAI and GP_{max} (e.g. Laurila *et al* 2001, Street *et al* 2007), however, provide strong support for the function that we chose for modeling the seasonal LAI patterns. Our simple model with DD as an environmental driver seemed to be suitable for our site and for this time period, but without cross-site validation it cannot be considered general, but rather a technical tool for local LAI estimation. Degree-day accumulation has found to be a reasonable driver of LAI in Arctic communities (e.g. Hollister *et al* 2005) and our model also included the effects of chilling temperatures in the latter part of the growing season. The phenological dynamics are also affected by the timing of thawing, thaw depth, previous year's conditions, soil moisture variations, herbivory, and photoperiod (Arft *et al* 1999, Marchand *et al* 2004, Körner and Basler 2010, Oberbauer *et al* 2013). These factors may be only partly accounted by the two-part DD model.

Our results show how the phenological stage of the vegetation can rapidly change in the short growing season of the Arctic and, therefore, that the timing of satellite image acquisition really matters. We illustrate how the spatial pattern of the LAI in the two images of the same area differ and how linking the vegetation patterns to the NDVI values of our QB image would result in a biased relationship and affect the interpretation of the remote-sensing products (Williams *et al* 2008, Ustin and Gamon 2010). VHSR satellite imagery is a significant improvement over traditional imagery, such as Landsat, for mapping the vegetation and associated processes of heterogeneous landscapes, such as tundra (Laidler and Treitz 2003, Virtanen and Ek 2014, Siewert *et al* 2015, Shrestha *et al* 2016). However, it is not unusual for these images to be acquired in different years or dates than the field data, because the availability of VHSR images of the Arctic is limited, due to infrequent satellite visits and unfavorable cloud conditions and zenith angles in these areas (Hope and Stow 1996, Rees *et al* 2002, Stow *et al* 2004, Westergaard-Nielsen *et al* 2013). Our data showt that one must be cautious in interpreting images without knowing the phenological stage of the most abundant plant species and communities at the time of imaging.

Moreover, these data add knowledge on arctic vegetation patterns and satellite derived NDVI in a less studied region in eastern Siberia representing a coastal

lowland middle Arctic tundra landscape. In order to spatially extrapolate LAI over the study area we applied an empirical relationship between plot scale LAI and VHRS NDVI with a typical exponential form (figure 5) observed across the Arctic (Van Wijk and Williams 2005, Stelzer and Welker 2006, Street *et al* 2007, Shaver *et al* 2007 and 2013, Williams *et al* 2008, Stoy *et al* 2009, Stoy and Quaife 2015). We found the relationship roughly similar between our study with VHSR derived NDVI and, for example, study by Shaver *et al* (2013) with multi-site data of field-spectrometer derived NDVI (figure 5(*d*)). However, similarities or differences in the NDVI-LAI relationship among sites and sensors deserve further attention, because it is commonly used for large scale extrapolations, but are known to be affected by changes in spatial scales (Spadavecchia *et al* 2008, Stoy *et al* 2009, Stoy and Quaife 2015, Williams *et al* 2008), between vegetation type or content (Stelzer and Welker 2006, Street *et al* 2007) and growing season (Street *et al* 2007). To our knowledge none of earlier studies has focused on similar Siberian calcareous tundra landscapes nor employed VHSR satellite imagery to establish LAI-NDVI relationship there. Data from multiple sites and including seasonal and multi-year variation would be valuable as verification material for developing models to generate LAI maps of the Arctic based on satellite images

Conclusions

Our objective was to determine the composition, distribution, and seasonal dynamics of the LAI in the plant communities of the arctic tundra and to assess how the seasonality of plant growth affects the interpretation of the vegetation signal derived from satellite images. Our observations have significant implications for the evaluation and planning of optical Earth observations and for compromising between spatial and temporal resolution. Understanding the small-scale spatial variation in plant communities, plant growth dynamics, and their constraints are highly important in heterogeneous landscapes when biological variables are interpreted, using VHSR Earth observation data. We conclude that the short growing season of high latitudes, in association with climatic variation, sets special requirements for linking non-matching field data and satellite images in these areas.

Acknowledgments

We thank Emmi Vähä and Lauri Rosenius for field and laboratory assistance, and James Thompson for English revision. This research was supported by the Academy of Finland (projects 269095 and 291736 for MA and TV). We thank G Chumachenko and O Dmitrieva for kindly making arrangements for our stay at the Tiksi Observatory and Yakutian Service for Hydrometeorology and Environmental Monitoring for providing accommodation and access to the observatory.

References

AARI 2016 Electronic archive AARI term meteorological and upper-air observations Hydrometeorological Observatory AARI 2016 (station) Tiksi for 1932−2014 (www.aari.ru/main.php?sub=2&id=3)

Arft A M *et al* 1999 Responses of tundra plants to experimental warming: meta-analysis of the international tundra experiment *Ecol. Monogr.* **69** 491–511

Bratsch S N, Epstein H E, Buchhorn M and Walker D A 2016 Differentiating among four arctic tundra plant communities at Ivotuk, Alaska using field spectroscopy *Rem. Sens.* **8** 51

Chapin F S III, Bret-Harte M S, Hobbie S E and Zhong H 1996 Plant functional types as predictors of transient responses of arctic vegetation to global change *J. Veg. Sci.* **7** 347–58

Chavez P S Jr 1988 An improved dark-object subtraction technique for atmospheric scattering correction of multispectral data *Rem. Sens. Environ.* **24** 459–79

Cramer W *et al* 2001 Global response of terrestrial ecosystem structure and function to CO_2 and climate change: results from six dynamic global vegetation models *Glob. Change Biol.* **7** 357–73

Forbes B C Macias Fauria M and Zetterberg P I 2010 Russian Arctic warming and 'greening' are closely tracked by tundra shrub willows *Glob. Change Biol.* **16** 1542–54

Frost G V and Epstein H E 2014 Tall shrub and tree expansion in Siberian tundra ecotones since the 1960s *Glob. Change Biol.* **20** 1264–77

Garrigues S *et al* 2008 Validation and intercomparison of global leaf area index products derived from remote sensing data *J. Geophys. Res.* **113** G02028

Hollister R D, Webber P J and Bay C 2005 Plant response to temperature in northern Alaska: implications for predicting vegetation change *Ecology* **86** 562–1570

Hope A S and Stow D A 1996 Shortwave reflectance properties of arctic tundra landscapes *Landscape Function and Disturbance in Arctic Tundra* ed J Reynolds and J Tenhunen (Berlin Heidelberg: Springer) pp 155–64

Hugelius G, Virtanen T, Kaverin D, Pastukhov A, Rivkin F, Marchenko S, Romanovsky V and Kuhry P 2011 High-resolution mapping of ecosystem carbon storage and potential effects of permafrost thaw in periglacial terrain, European Russian Arctic *J. Geophys. Res.* **116** G03024

Johnson D A and Tieszen L L 1976 Aboveground biomass allocation, leaf growth, and photosynthesis patterns in tundra plant forms in Arctic Alaska *Oecologia* **24** 159–73

Körner C and Basler D 2010 Phenology under global warming *Science* **327** 1461–2

Laidler G J and Treitz P 2003 Biophysical remote sensing of arctic environments *Progr. Phys. Geogr.* **27** 44–68

Laidler G, Treitz P and Atkinson D 2008 Remote sensing of arctic vegetation: relations between the NDVI, spatial resolution and vegetation cover on Boothia Peninsula, Nunavut *Arctic* **61** 1–13

Laurila T, Soegaard H, Lloyd C R, Aurela M, Tuovinen J-P and Nordstroem C 2001 Seasonal variations of net CO_2 exchange in European Arctic ecosystems *Theor. Appl. Climatol.* **70** 183–201

Maanavilja L, Riutta T, Aurela M, Laurila T and Tuittila E-S 2010 Spatial variation in CO_2 exchange at a northern aapa mire *Biogeochemistry* **104** 325–45

Marchand F L, Nijs I, Heuer M, Mertens S, Kockelberh I, Pontailler J-Y, Impens I and Beyens L 2004 Climatic warming responses of high arctic tundra *Arct. Antarct. Alp. Res.* **36** 390–4

Marushchak M E, Kiepe I, Biasi C, Elsakov V, Friborg T, Johansson T, Soegaard H, Virtanen T and Martikainen P 2013 Carbon dioxide balance of subarctic tundra from plot to regional scales *Biogeosciences* **10** 437–52

McManus K M, Morton D C, Masek J G, Wang D, Sexton J O, Nagol J R, Ropars P and Boudreau S 2012 Satellite-based evidence for shrub and graminoid tundra expansion in northern Quebec from 1986 to 2010 *Glob. Change Biol.* **18** 2313–23

Melton J R *et al* 2013 Present state of global wetland extent and wetland methane modelling: conclusions from a model inter-comparison project (WETCHIMP) *Biogeosciences* **10** 753–88

Moore T R, Lafleur P M, Poon D M, Heuman B W, Seaquist J W and Roulet N T 2006 Spring photosynthesis in a cool temperate bog *Glob. Change Biol.* **12** 2323–35

Mora C, Vieira G, Pina P, Lousada M and Christiansen H H 2015 Land cover classification csing high-resolution aerial photography in Adventdalen, Svalbard *Geogr. Ann. Ser. A: Phys. Geog.* **97** 473–88

Oberbauer S F *et al* 2013 Phenological response of tundra plants to background climate variation tested using the international tundra experiment *Phil. Trans. R. Soc.* B **368** 20120481

Rautiainen M, Mõttus M, Heiskanen J, Akujärvi A, Majasalmi T and Stenberg P 2011 Seasonal reflectance dynamics of common understory types in a northern european boreal forest *Rem. Sens. Environ.* **115** 3020–8

Rees G, Brown I, Mikkola K, Virtanen T and Werkman B 2002 How can the dynamics of the tundra-taiga boundary be remotely monitored? *Ambio Spec. Rep.* **12** 56–62

Riutta T, Laine J and Tuittila E-S 2007 Sensitivity of CO_2 exchange of fen ecosystem components to water level variation *Ecosystems* **10** 718–33

Saarinen T 1998 Demography of carex rostrata in a boreal mesotrophic fen: shoot dynamics and biomass development *Ann. Bot. Fenn.* **35** 203–9

Shaver G R, Street L E, Rastetter E B, Van Wijk M T and Williams M 2007 Functional convergence in regulation of net CO_2 flux in heterogeneous tundra landscapes in Alaska and Sweden *J. Ecol.* **95** 802–17

Shaver G R, Rastetter E B, Salmon V, Street L E, van de Weg M J, Rocha A, van Wijk M T and Williams M 2013 Pan-arctic modelling of net ecosystem exchange of CO_2 *Phil. Trans. R. Soc.* B **368** 20120485

Shrestha R K, Arora V K and Melton J R 2016 The sensitivity of simulated competition between different plant functional types to subgrid-scale representation of vegetation in a land surface model *J. Geophys. Res.-Biogeosci.* **121** 809–28

Siewert M B, Hanisch J, Weiss N, Kuhry P, Maximov T C and Hugelius G 2015 Comparing carbon storage of siberian tundra and taiga permafrost ecosystems at very high spatial resolution *J. Geophys. Res.-Biogeosci.* **120** 1973–94

Spadavecchia L, Williams M, Bell R, Stoy P C, Huntley B and Van Wijk M T 2008 Topographic controls on the leaf area index and plant functional type of a tundra ecosystem *J. Ecol.* **96** 1238–51

Stelzer H and Welker J M 2006 Modeling the effect of photosynthetic vegetation properties on the NDVI-LAI relationship *Ecology* **87** 2765–72

Stow D A *et al* 2004 Remote sensing of vegetation and land-cover change in arctic tundra ecosystems *Rem. Sens. Environ.* **89** 281–308

Stoy P C and Quaife T 2015 Probabilistic downscaling of remote sensing data with applications for multi-scale biogeochemical flux modeling *PLoS ONE* **10** e0128935

Stoy P C, Williams M, Spadavecchia L, Bell R A, Prieto-Blanco A, Evans J G and Van Wijk M T 2009 Using information theory to determine optimum pixel size and shape for ecological studies: aggregating land surface characteristics in arctic ecosystems *Ecosystems* **12** 574–89

Street L E, Shaver G R, Williams M and Van Wijk M T 2007 What is the relationship between changes in canopy leaf area and changes in photosynthetic CO_2 flux in arctic ecosystems? *J. Ecol.* **95** 139–50

Street L E, Stoy P C, Sommerkorn M, Fletcher B J, Sloan V L, Hill T C and Williams M 2012 Seasonal bryophyte productivity in the sub-arctic: a comparison with vascular plants *Funct. Ecol.* **26** 365–78

Tieszen L L and Johnson P L 1968 Pigment structure of some arctic tundra communities *Ecology* **49** 370–373

Tucker C J 1979 Red and photographic infrared linear combinations for monitoring vegetation *Rem. Sens. Environ.* **8** 127–50

Ustin S L and Gamon J A 2010 Remote sensing of plant functional types *New Phytol.* **186** 795–816

Uttal T *et al* 2016 International arctic systems for observing the atmosphere (IASOA): an international polar year legacy consortium *Bull. Am. Meteorol. Soc.* **97** 1033–56

Van Wijk M T and Williams M 2005 Optical instruments for measuring leaf area index in low vegetation: application in Arctic ecosystems *Ecol. Appl.* **15** 1462–70

Virtanen T and Ek M 2014 The fragmented nature of tundra landscape *Int. J. Appl. Earth Obs. Geoinf.* **27** 4–12

Vogelmann J E and Moss D E 1993 Spectral reflectance measurements in the genus Sphagnum *Rem. Sens. Environ.* **45** 273–9

Westergaard-Nielsen A, Lund M, Hansen B U and Tamstorf M P 2013 Camera derived vegetation greenness index as proxy for gross primary production in a low Arctic wetland area *ISPRS J. Photogramm. Rem. Sens.* **86** 89–99

Williams M, Bell R, Spadavecchia L, Street L E and van Wijk M T 2008 Upscaling leaf area index in an Arctic landscape through multiscale observations *Glob. Change Biol.* **14** 1517–30